# Heat transfer and solidification of a laminar liquid flow in a cooled parallel plate channel: The stationary case

B. Weigand and H. Beer, Darmstadt, BRD

**Abstract.** A simple numerical model is presented to predict the steady-state ice layers on the cooled walls inside a parallel plate channel for arbitrary entrance velocity profiles. The effect of two different entrance velocity distributions (a parabolic velocity distribution and a slug flow) on the shape of the ice-layers are examined. The quality of an approximative solution given in literature was checked by comparing with the numerical results. For the case of a fully developed parabolic velocity distribution at the entrance of the cooled channel the results are compared with experimental findings of Kikuchi [8]. A generally good agreement was found.

### Erstarren einer laminar strömenden Flüssigkeit in einem ebenen Kanal: Der stationäre Zustand

**Zusammenfassung.** Es wurde ein einfaches numerisches Modell entwickelt, das es ermöglicht, die stationären Erstarrungsfronten an den Kanalwänden für beliebige Verteilungen des Eintrittsgeschwindigkeitsprofils zu berechnen. Als Beispiele wurden ein voll ausgebildetes Parabelprofil und ein Pfropfenprofil am Eintritt in die Kühlstrecke untersucht. Mit Hilfe der numerischen Lösung konnte die Güte einer aus der Literatur bekannten Näherungslösung zur Berechnung der Erstarrungsfronten überprüft werden. Für den Fall des Parabelprofils am Kanaleintritt wurde die Rechnung mit Meßwerten von Kikuchi [8] verglichen. Es zeigte sich eine gute Übereinstimmung zwischen Theorie und Experiment.

## Nomenclature

| | |
|---|---|
| $a$ | thermal diffusivity |
| $B$ | dimensionless freezing parameter [Eq. (30)] |
| $D$ | hydraulic diameter: $D = 4h$ |
| $F, f$ | modified stream functions |
| $h$ | distance from centerline to the wall |
| $k$ | thermal conductivity |
| $Nu$ | local Nusselt number |
| $P$ | pressure |
| $Pr$ | Prandtl number |
| $Re_h$ | Reynolds number based on $h$ |
| $Re_D$ | Reynolds number based on the hydraulic diameter |
| $T$ | temperature |
| $T_b$ | bulk temperature |
| $T_F$ | freezing temperature of the liquid |
| $T_0$ | constant inlet temperature of the liquid |
| $u, v$ | fluid velocity components |
| $\bar{u}$ | mean axial velocity |
| $u_{max}$ | maximum axial velocity at the channel centerline |
| $x, y$ | coordinates |
| $\delta$ | distance from centerline to the liquid-solid interface |

| | |
|---|---|
| $\theta_W$ | dimensionless temperature difference [Eq. (30)] |
| $\varrho$ | density |
| $v$ | kinematic viscosity |
| $\psi$ | stream function |

*Subscripts*

| | |
|---|---|
| $s$ | solid |
| $L$ | liquid |
| $w$ | at the wall |
| $0$ | at the entrance |

*Superscripts*

| | |
|---|---|
| $\sim, *$ | dimensionless quantity |

## 1 Introduction

Problems of solidification or freezing of liquids flowing through channels have been encountered in numerous engineering applications. Because a freeze shut may lead to a destruction of the system (water pipe, heat exchanger, molten sodium in a nuclear reactor) blockage should be prevented. If solidification on the cooled channel walls can not be suppressed, steady state conditions must be aimed.

Many theoretical and experimental studies have been performed for fluid flow with solidification in circular tubes. An early investigation was reported by Zerkle and Sunderland [1] for the steady-state freezing of laminar flow inside a horizontal tube. Under the assumption of a parabolic axial velocity distribution throughout the full axial region and with an appropriate coordinate transformation, they were able to reduce the problem to the classical Graetz problem without solidification. Özisik and Mulligan [2] used a slug flow approximation for the liquid core to analyze transient solidification in an isothermal circular tube. They applied integral transforms to obtain the transient development of the ice-layer inside the tube. Bilenas and Jiji [3] solved the boundary-layer equations applying a finite-difference scheme, but used a wide-meshed grid for their calculation. Chida [4] calculated numerically, under consideration of axial conduction, the steady state ice-layer thickness. A fully developed

parabolic axial velocity distribution at the entrance of the cooled section was assumed in [3] and [4]. The combined thermal and hydrodynamic development during solidification inside an isothermal tube has been analyzed by Hwang and Sheu [5]. Under the assumption that the axial variation of the solid layer thickness was small, they were able to reduce the problem to the combined entry region problem without solidification. The simplifications made in [5] give accurate solutions only for small dimensionless freezing parameters $(B \leqslant 3)$.

Despite its relevance to many important technological and physical problems, the freezing of liquid flows through a cooled two dimensional channel has scarely been studied, both, analytically and experimentally. An early investigation of this problem was reported by Lee and Zerkle [6]. They assumed the axial velocity distribution to be parabolic throughout the chill region, which was in analogy to [1]. With this assumption, the axial velocity distribution yields

$$\frac{u}{\bar{u}} = \frac{3}{2}\left[1-\left(\frac{y}{\delta}\right)^2\right]; \quad \bar{u} = \frac{\bar{u}_0\, h}{\delta} \quad (1)$$

With the approximated velocity profile according to Eq. (1) and with an appropriate coordinate transformation, the energy equation could then be reduced to a Graetz problem and the steady-state ice layer was calculated. Cheng and Wong [7] extended the model used in [6] to calculate the influence of an externally imposed convective boundary condition on the ice-layer.

Bennon and Incropera [9] studied numerically the influence of free convection effects on the axial distribution of the solid-liquid interface in a cooled channel with laminar flow for a fully developed parabolic entrance velocity profile. An experimental investigation of the effect of freezing of liquid for laminar flow between two cooled parallel plates was only performed by Kikuchi et al. [8]. Both plates were maintained at the same temperature, which was lower than the freezing temperature of the working fluid, water. The plate wall temperature varied from $-2\,°\mathrm{C}$ to $-7\,°\mathrm{C}$.

The subject of this paper is the presentation of a simple numerical model for the prediction of the steady-state ice layers inside a two-dimensional channel with cooled walls for arbitrary velocity profiles at the entrance of the chill section. Two entrance velocity profiles will be examined:

- fully developed parabolic velocity distribution
- slug flow

The numerical results are used to check the approximative solution given in literature for a fully developed entrance profile [6].

## 2 Analysis

### 2.1 Formulation of the problem

Figure 1 shows the geometrical configuration and the coordinate system for a planar symmetric channel. The laminar
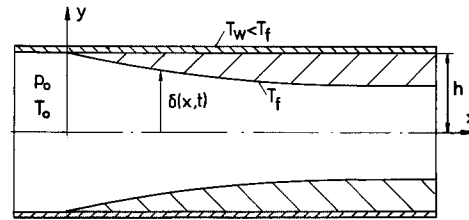
Fig. 1. Physical model and coordinate system

fluid flow enters the cooled section at $x=0$ with an arbitrary velocity profile and with constant temperature $T_0$. In the cooled section $(x>0)$ the wall temperature is maintained at a constant value $T_W$ which is lower than the freezing temperature $T_F$ of the fluid. The frozen layers are generated on both walls as the fluid proceeds along the channel. By assuming an incompressible, Newtonian fluid with constant fluid properties, the quasi-steady conservation equations for the fluid may be written as follows:

$$\frac{\partial u}{\partial x} + \frac{\partial v}{\partial y} = 0 \quad (2)$$

$$u\frac{\partial u}{\partial x} + v\frac{\partial u}{\partial y} = -\frac{1}{\varrho}\frac{\partial p}{\partial x} + v\frac{\partial^2 u}{\partial y^2} \quad (3)$$

$$u\frac{\partial T_L}{\partial x} + v\frac{\partial T_L}{\partial y} = a\frac{\partial^2 T_L}{\partial y^2} \quad (4)$$

By deriving the Eqs. (2)–(4) the usual boundary-layer assumptions were made, which are a common treatment of the conservation equations for channel flows [3], [10], [11].

In addition to Eqs. (2)–(4), the energy equation for the solid region is required. By assuming constant properties in the solid region and negligible axial conduction, the heat conduction equation for the solid-phase reduces to

$$\frac{\partial^2 T_s}{\partial y^2} = 0 \quad (5)$$

After neglecting the momentum equation in $y$-direction, the presence of $\partial p/\partial x$ in Eq. (3) introduces an additional unknown to the system given by Eqs. (2)–(4). Thus another equation is required. It is provided by the conservation of mass in integral form for steady state conditions

$$\bar{u}_0\, h = \int_0^\delta u\, dy \quad (6)$$

where $\bar{u}_0$ is the mean axial velocity for $x=0$.

The boundary conditions belonging to Eq. (2)–(5) are:

$$x = 0: \quad p = p_0, \quad u = \text{given}, \quad v = \text{given}, \quad T = T_0$$

$$y = 0: \quad \frac{\partial T_L}{\partial y} = 0; \quad \frac{\partial u}{\partial y} = 0; \quad v = 0$$

$$y = \delta: \quad u = v = 0; \quad T_L = T_F; \quad T_s = T_F$$

$$y = h: \quad T_s = T_w \quad (7)$$

Eqs. (2)–(4) and (5) are coupled by the interface energy equation which takes the following form if curvature terms are neglected:

$$k_s \frac{\partial T_s}{\partial y} - k_L \frac{\partial T_L}{\partial y} = \varrho_s r_s \frac{\partial \delta}{\partial t} \; ; \quad y = \delta \tag{8}$$

Equation (8) shows that the heat conducted in the solid plus the heat resulting from phase change equals the heat transport from the liquid. For steady-state conditions Eq. (8) simplifies to:

$$k_s \frac{\partial T_s}{\partial y} = k_L \frac{\partial T_L}{\partial y} \; ; \quad y = \delta \tag{9}$$

### 2.2 Temperature distribution in the solid region

With the boundary conditions Eq. (7) the temperature distribution in the solid phase is easily calculated from Eq. (5).

$$T_s = \frac{T_w (y - \delta) + T_F (h - y)}{h - \delta} \tag{10}$$

Inserting Eq. (10) into Eq. (9) results in:

$$\left. \frac{\partial T_L}{\partial y} \right|_{y=\delta} = \frac{k_s}{k_L} \frac{T_w - T_F}{h - \delta} \tag{11}$$

### 2.3 Velocity and temperature distribution in the liquid

Introducing the following dimensionless quantities into Eqs. (2)–(4)

$$u^* = \frac{u}{\bar{u}_0} \; ; \quad v^* = \frac{v}{\bar{u}_0} \sqrt{Re_h} \; ; \quad Re_h = \frac{\bar{u}_0 h}{\nu} \; ; \quad \theta = \frac{T - T_F}{T_0 - T_F}$$

$$x^* = \frac{x}{h} \; ; \quad y^* = \frac{y}{h} \sqrt{Re_h} \tag{12}$$

results in the ensueing set of equations:

$$\frac{\partial u^*}{\partial x^*} + \frac{\partial v^*}{\partial y^*} = 0 \tag{13}$$

$$u^* \frac{\partial u^*}{\partial x^*} + v^* \frac{\partial u^*}{\partial y^*} = -\frac{dp^*}{dx^*} + \frac{\partial^2 u^*}{\partial y^{*2}} \tag{14}$$

$$u^* \frac{\partial \theta}{\partial x^*} + v^* \frac{\partial \theta}{\partial y^*} = \frac{1}{Pr} \frac{\partial^2 \theta}{\partial y^{*2}} \tag{15}$$

Introducing a stream function, defined as

$$u^* = -\frac{\partial \psi}{\partial y^*} \; ; \quad v^* = \frac{\partial \psi}{\partial x^*} \tag{16}$$

Equations (13)–(15) may be written as:

$$\frac{\partial \psi}{\partial y^*} \frac{\partial^2 \psi}{\partial x^* \partial y^*} - \frac{\partial \psi}{\partial x^*} \frac{\partial^2 \psi}{\partial y^{*2}} = -\frac{dp^*}{dx^*} - \frac{\partial^3 \psi}{\partial y^{*3}} \tag{17}$$

$$-\frac{\partial \psi}{\partial y^*} \frac{\partial \theta}{\partial x^*} - \frac{\partial \psi}{\partial x^*} \frac{\partial \theta}{\partial y^*} = \frac{1}{Pr} \frac{\partial^2 \theta}{\partial y^{*2}} \tag{18}$$

Because the boundary conditions of Eqs. (17) and (18) must be satisfied for $y = \delta$, it is useful to employ the following coordinate transformation

$$\tilde{y} = \sqrt{Re_h} - \frac{y^*}{\delta^*} \; ; \quad \tilde{x} = x^* \tag{19}$$

with $\delta^* = \delta/h$. A transform similar to Eq. (19) was first used in [1] with the purpose of reducing the energy equation to the Graetz problem without solidification.

Applying the coordinate transform to Eqs. (17), (18), and inserting a modified stream function according to

$$\psi = \delta^* F(\tilde{x}, \tilde{y}) , \tag{20}$$

results in the following system of partial differential equations

$$\frac{1}{\delta^{*2}} \frac{\partial^3 F}{\partial \tilde{y}^3} = \frac{dp^*}{d\tilde{x}} + \frac{\partial F}{\partial \tilde{y}} \frac{\partial^2 F}{\partial \tilde{x} \partial \tilde{y}} - \frac{\partial F}{\partial \tilde{x}} \frac{\partial^2 F}{\partial \tilde{y}^2} - \underline{\frac{1}{\delta^*} \frac{d\delta^*}{d\tilde{x}} F \frac{\partial^2 F}{\partial \tilde{y}^2}} \tag{21}$$

$$\frac{1}{\delta^{*2}} \frac{\partial^2 \theta}{\partial \tilde{y}^2} = Pr \left( \frac{\partial F}{\partial \tilde{y}} \frac{\partial \theta}{\partial \tilde{x}} - \frac{\partial F}{\partial \tilde{x}} \frac{\partial \theta}{\partial \tilde{y}} - \underline{\frac{1}{\delta^*} \frac{d\delta^*}{d\tilde{x}} F \frac{\partial \theta}{\partial \tilde{y}}} \right) \tag{22}$$

The term $1/\delta^{*2}$ on the left side of Eqs. (21) and (22) could easily be eliminated by invoking a new axial coordinate, defined as

$$\xi = \int_0^{\tilde{x}} \frac{1}{\delta^{*2}} d\tilde{x}$$

However, this will not be done, because it offers no advantage in solving Eqs. (21), (22) numerically. Nevertheless, it is very interesting to see, that the transformation of a channel with a variable distance between the walls $\delta^*(\tilde{x})$, into a channel with parallel walls in $\xi, \tilde{y}$ coordinates, will introduce only one additional term into the conservation equations. This term, which is underlined in Eqs. (21) and (22), represents the effect of acceleration which results from converging ice-layers in the axial direction.

Equations (21) and (22) were derived in physical coordinates which are appropriate in the case of a fully developed parabolic axial velocity profile at the entrance of the chill region. For the case of combined hydrodynamic and thermal development of the flow, which is given by a slug flow profile at the entrance of the cooling section, however, it is convenient to take Falkner-Skan transformed variables [9]:

$$\eta = \frac{\tilde{y}}{\sqrt{\tilde{x}}} \; ; \quad \tilde{x} = \tilde{x} \tag{23}$$

The coordinates defined by Eq. (23), stretch the thin near wall region of the boundary layer. Because of this fact, it is possible to calculate the velocity- and temperature distribution in the entrance region of the channel very effectively. After the velocity- or thermal-boundary layer thickness becomes approximately 75% of the distance from channel centerline to solid-liquid interface, the coordinates were changed and the calculations were performed with the variables given by Eq. (19).

Applying the coordinate transform to the conservation equations and inserting a modified stream-function

$$F(\tilde{x}, \tilde{y}) = \sqrt{\tilde{x}} \, f(\tilde{x}, \eta) \tag{24}$$

eqs. (21) and (22) can be written in the following form:

$$\frac{1}{\delta^{*2}} \frac{\partial^3 f}{\partial \eta^3} + \frac{1}{2} f \frac{\partial^2 f}{\partial \eta^2} = \tilde{x} \frac{dp^*}{d\tilde{x}} + \tilde{x} \left( \frac{\partial f}{\partial \eta} \frac{\partial^2 f}{\partial \tilde{x} \partial \eta} - \frac{\partial f}{\partial \tilde{x}} \frac{\partial^2 f}{\partial \eta^2} \right.$$
$$\left. - \frac{1}{\delta^*} \frac{d\delta^*}{d\tilde{x}} f \frac{\partial^2 f}{\partial \eta^2} \right) \tag{25}$$

$$\frac{1}{\delta^{*2}} \frac{\partial^2 \theta}{\partial \eta^2} + \frac{Pr}{2} f \frac{\partial \theta}{\partial \eta} = Pr \, \tilde{x} \left( \frac{\partial f}{\partial \eta} \frac{\partial \theta}{\partial \tilde{x}} - \frac{\partial \theta}{\partial \eta} \frac{\partial f}{\partial \tilde{x}} - \frac{1}{\delta^*} \frac{d\delta^*}{d\tilde{x}} f \frac{\partial \theta}{\partial \eta} \right) \tag{26}$$

The boundary conditions for Eqs. (21) and (22) or Eqs. (25) and (26) are given by:

$\tilde{x} = 0$: $\theta = 1$, $F =$ given        $\tilde{x} = 0$: $\theta = 1$, $f =$ given

$\tilde{y} = 0$: $F = \partial F / \partial \tilde{y} = 0$, $\theta = 0$    $\eta = 0$: $f = \partial f / \partial \eta = 0$, $\theta = 0$

$\tilde{y} = \sqrt{Re_h}$: $\partial^2 F / \partial \tilde{y}^2 = 0$, $\partial \theta / \partial \tilde{y} = 0$

$$\eta = \frac{\sqrt{Re_h}}{\sqrt{\tilde{x}}}: \quad \frac{\partial^2 f}{\partial \eta^2} = 0; \quad \frac{\partial \theta}{\partial \eta} = 0 \tag{27}$$

The energy balance at the liquid-solid interface, Eq. (11), expressed in physical coordinates, is given by

$$\frac{\sqrt{Re_h}}{B} \left. \frac{\partial \theta}{\partial \tilde{y}} \right|_{\tilde{y}=0} = \frac{\delta^*}{1 - \delta^*} \tag{28}$$

and in transformed variables

$$\frac{\sqrt{Re_h}}{\sqrt{\tilde{x}}} \frac{1}{B} \left. \frac{\partial \theta}{\partial \eta} \right|_{\eta=0} = \frac{\delta^*}{1 - \delta^*} \tag{29}$$

with the dimensionless freezing parameter $B$, defined as

$$B = \frac{k_s}{k_L} \frac{T_F - T_W}{T_0 - T_F} = \frac{k_s}{k_L} \theta_W \tag{30}$$

## 3 Calculation of the solid-liquid interface

The calculation of the frozen layer can be performed in the following manner: An arbitrary distribution for $\delta^*(\tilde{x})$ is assumed, for example a linear decreasing function of $\tilde{x}$. With the assumed distribution of $\delta^*(\tilde{x})$ Eqs. (21)–(22) or Eqs. (25)–(26) can be solved numerically according to the boundary conditions given by Eq. (27). After solving the conservation equations, a new distribution of $\delta^*(\tilde{x})$ is calculated by inserting the yet known temperature gradient at the solid-liquid interface into Eq. (28) or Eq. (29). The procedure described above results in an iteration scheme which converges rapidly. Normally only three iterations are needed to get $\delta^*(\tilde{x})$ with sufficient accuracy.

### 3.1 The numerical method

In order to obtain solutions for example of Eqs. (21) and (22) with the boundary conditions Eq. (27), an implicit finite-difference method is applied, which is known in literature as the Keller-box method. A detailed description can be found in [10] and [11]. Because the box scheme is a common method to solve parabolic differential equations, only a brief outline is provided here. In consequence of the assumption of an incompressible fluid with constant properties, the equation of motion and the energy equation are uncoupled and may be solved separately.

#### 3.1.1 The velocity distribution

The momentum Eq. (21) will be first reduced to a first-order system of differential equations

$$\frac{\partial F}{\partial \tilde{y}} = U \tag{31}$$

$$\frac{\partial U}{\partial \tilde{y}} = V \tag{32}$$

$$\frac{1}{\delta^{*2}} \frac{\partial V}{\partial \tilde{y}} = \frac{dp^*}{d\tilde{x}} + U \frac{\partial U}{\partial \tilde{x}} - V \frac{\partial F}{\partial \tilde{x}} - \frac{1}{\delta^*} \frac{d\delta^*}{d\tilde{x}} FV \tag{33}$$

The following boundary conditions belong to Eqs. (31)–(33)

$\tilde{x} = 0$,    $F =$ given

$\tilde{y} = 0$,    $F = U = 0$

$\tilde{y} = \sqrt{Re_h}$,    $V = 0$ \hfill (34)

The conservation equation in integral form, Eq. (6), has to be satisfied. Inserting the definition of the stream-function into Eq. (6), results in

$$\tilde{y} = \sqrt{Re_h}, \quad F = \frac{\sqrt{Re_h}}{\delta^*} \tag{35}$$

For $0 \le \tilde{x} \le \tilde{x}_N$ und $0 \le \tilde{y} \le \sqrt{Re_h}$ a possibly nonuniform net is placed

$\tilde{x}_0 = 0$,    $\tilde{x}_n = \tilde{x}_{n-1} + k_n$;    $n = 1, 2, \dots, N$ \hfill (36)

$\tilde{y}_0 = 0$,    $\tilde{y}_j = \tilde{y}_{j-1} + h_j$;    $j = 1, 2, \dots, J, \tilde{y}_J = \sqrt{Re_h}$

with $k_n$ and $h_j$ denoting variable distances between nodes in the $\tilde{x}$ and $\tilde{y}$ direction. Equations (31) and (32) were approximated by central-difference quotients and averages about the midpoint $(\tilde{x}_n, \tilde{y}_{j-1/2})$, while Eq. (33) was centered about the midpoint $(\tilde{x}_{n-1/2}, \tilde{y}_{j-1/2})$. After approximating the boundary conditions, Eq. (34), with central difference quotients, a system of $3J + 3$ nonlinear equations for the $3J + 3$ unknowns $(F_j^n, U_j^n, V_j^n)$ is obtained. The system can easily be solved by block elimination after linearization by applying Newton's method. The pressure gradient appearing in Eq. (33) was treated as a nonlinear eigenvalue. Details of the numerical method are found in [10].

### 3.1.2 The temperature distribution

The method used to obtain solutions of Eq. (22) is similar to that described in the previous section. Reducing Eq. (22) to a first order system of differential equations yields

$$\frac{\partial \theta}{\partial \tilde{y}} = P \tag{37}$$

$$\frac{1}{\delta^{*2}} \frac{\partial P}{\partial \tilde{y}} = Pr \left( U \frac{\partial \theta}{\partial \tilde{x}} - P \frac{\partial F}{\partial \tilde{x}} - \frac{1}{\delta^*} \frac{d\delta^*}{d\tilde{x}} FP \right) \tag{38}$$

with the boundary conditions

$$\tilde{x} = 0: \quad \theta = 1$$
$$\tilde{y} = 0: \quad \theta = 0 \tag{39}$$
$$\tilde{y} = \sqrt{Re_h}: \quad P = 0$$

Equation (37) was approximated by central-difference quotients and averages about the midpoint $(\tilde{x}_n, \tilde{y}_{j-1/2})$, while Eq. (38) was centered about the midpoint $(\tilde{x}_{n-1/2}, \tilde{y}_{j-1/2})$ using the same net defined by Eq. (36). The solution of the resulting linear system of equations was obtained by the same block elimination method used with the momentum equation.

### 3.2 The solid-liquid interface

After solving Eqs. (37) and (38), the temperature gradient at the solid-liquid interface is known. Therefore, the distance between channel centerline and liquid-solid interface can be calculated from Eq. (28) for every axial position.

$$\delta^*_{(1)} = \frac{\sqrt{Re_h} \, P_W/B}{1 + \frac{\sqrt{Re_h}}{B} P_W} \tag{40}$$

After introducing this new distribution of $\delta^*(\tilde{x})$ into Eqs. (21) and (22), the velocity- and temperature distribution in the fluid can be calculated again. This results in the new distribution $\delta^*_{(2)}(\tilde{x})$. The iteration procedure described above was repeated until the deviation was within $\Delta\delta = |\delta^*_{(1)} - \delta^*_{(2)}| < 0.01$ for every axial position.

The iteration process converges rapidly. Normally only three iterations were necessary to get $\delta^*(\tilde{x})$ within the error tolerance given above. However, combined hydrodynamic and thermal development of the flow and large values of $B$ required some more iterations, but they did not exceed the number of ten.

## 4 Results and discussion

### 4.1 Parabolic entrance velocity profile

For the case of a fully developed parabolic velocity distribution at the entrance of the chill region, measurements were performed by Kikuchi et al. [8] with water. Figure 2 shows the effect of increasing wall cooling on the ice-layer at the
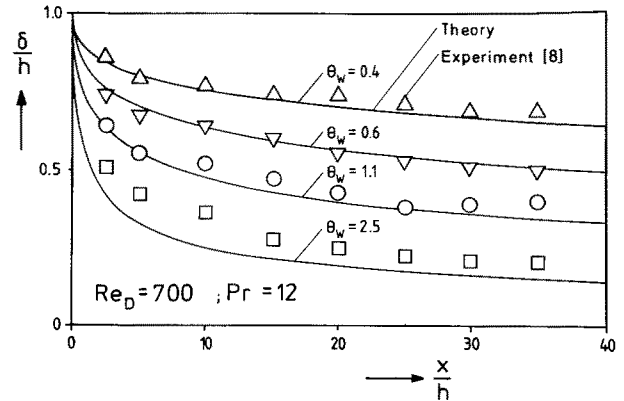
**Fig. 2.** Dimensionless distance from channel centerline to liquid-solid interface versus axial position for various $\theta_W$
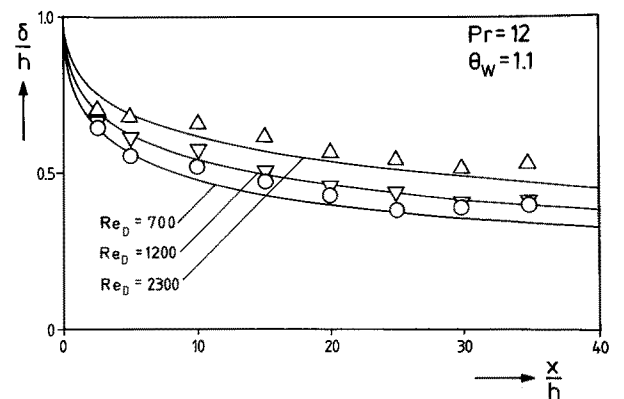
**Fig. 3.** Effect of Reynolds number on the axial distribution of $\delta^*$

wall for $Re_D = 700$ and $Pr = 12$, compared with experimental results of [8]. It is obvious that the ice-layer thickness increases rapidly with growing $\theta_W$. Generally the calculated distributions of $\delta^*(\tilde{x})$ are in good agreement with experimental findings, except for $\theta_W = 2.5$. The reason might be, that $\theta_W$ in [8] was given only by the axial mean value of the measured wall temperature. As the ice layer thickness reacts very sensitively on variations of $\theta_W$, a possibly nonuniform distribution of $\theta_W$ in the experiments could be responsible for the deviations from theory. Unfortunately, in [8] no comments are given about the uniformity of the wall temperature.

Figure 3 elucidates the influence of the Reynolds number on the axial distribution of $\delta^*$ for $\theta_W = 1.1$ and $Pr = 12$. The calculated results agree well with measured values of [8]. It can be seen that increasing Reynolds numbers results in growing heat flux from the fluid to the solid-liquid interface and therefore in a decreasing ice-layer thickness.

It is of importance to know the range of the dimensionless freezing parameter $B$ in which an approximation given by Lee and Zerkle [6] coincides well with the numerical results. In this approximation the axial velocity distribution was assumed to remain parabolic, according to Eq. (1), throughout the chill region. Figure 4 depicts a comparison between
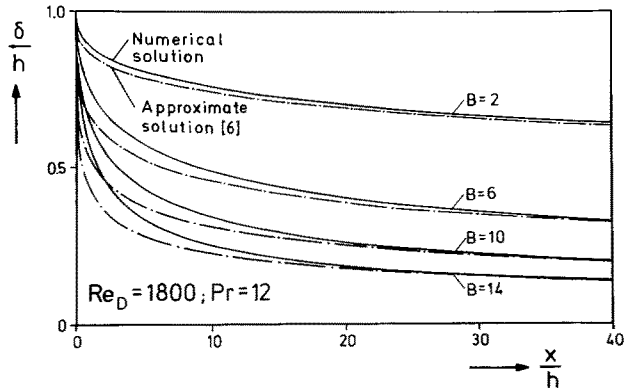
Fig. 4. Ice-layer thickness as a function of $x/h$ with $B$ as parameter, compared with the approximation given by Lee and Zerkle [6]
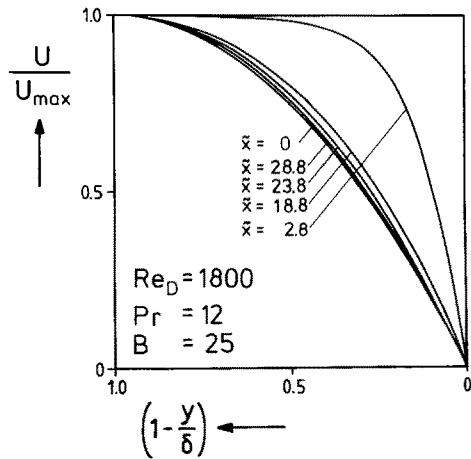


Fig. 6. Nusselt number as a function of $x/h$ with $\theta_W$ as parameter



Fig. 5. Axial velocity distribution as a function of $y/\delta$ for various $x/h$

steeper than for a parabolic profile ($\tilde{x}=2.8$). For increasing $\tilde{x}$ the axial change in ice-layer thickness decreases and the profile tends to a parabolic distribution. Because of this fact, the numerical calculation coincides with the approx. [6] for great values of $\tilde{x}$. This is also elucidated in Fig. 4.

Figure 6 illustrates the effect of increasing $\theta_W$ on the local Nusselt number $Nu$ for $Re_D = 700$ and $Pr = 12$. The Nusselt number is defined by

$$Nu = \frac{4\delta \left.\dfrac{\partial T}{\partial y}\right|_w}{T_F - T_b}.$$

$Nu$ first decreases rapidly with increasing $\tilde{x}$ and then approaches the value for a fully developed flow. It is obvious that the Nusselt number is but slightly effected by a variation in $\theta_W$.

## 4.2 Combined hydrodynamic- and thermal development

The combined hydrodynamic and thermal development during solidification is more complicated than solidification in the presence of a fully developed parabolic velocity profile. The acceleration of the fluid, caused by the converging ice-layers, gives rise to a more rapid development of the entering slug flow profile than in a channel without solidification. The velocity profile in the entrance region of combined hydrodynamic and thermal development has a much steeper gradient at the wall than for a fully developed profile at the entrance of the chill region. This results in an enhancement of the heat transfer between the liquid and the solid region and, therefore, in a thinner ice layer at the wall.

Figure 7 shows the axial distribution of $\delta^*$ for $Re_D = 400$, $Pr = 10$ and $B = 2$. Figures 8 and 9 illustrate the effect of acceleration due to the converging ice-layer of Fig. 7 on the axial velocity distribution. In Fig. 8 the velocity is scaled with $\bar{u}_0$, while in Fig. 9 $u$ is scaled by the maximum velocity $u_{max}$ at the channel centerline. Figure 9 elucidates the axial development of the velocity profile. For $\tilde{x} = 10$ the profile has adopted a nearly parabolic distribution.

the numerically calculated ice layers and freezing fronts which were determined by the approximation according to [6]. It can be seen, that the numerical solution leads to thinner ice layers than the approximative solution. This fact is due to the acceleration of the fluid according to the converging ice layers, which enhances heat transfer from the fluid to the solid-liquid interface and which inevitably is not taken into consideration in the approximation. The axial distribution of $\delta^*(\tilde{x})$ shows that the approx. [6] should not be used for high wall cooling parameters, e.g. $B \geqslant 10$, as it leads to a distinct deviation. The effect of acceleration, due to the converging ice-layers is visualized in Fig. 5 for $Re_D = 1800$ and $B = 25$. The velocity profiles show, that there is a great deviation between numerically calculated profiles and the velocity distribution according to Eq. (1). The difference between the parabolic distribution and the calculated velocity profiles is maximum for low values of $\tilde{x}$, because the axial change in the ice-layer thickness and, therefore, the acceleration of the fluid is large. The parabolic entrance velocity profile is strongly deformed in the entrance region of the chill section. The profile is flattened in the near core region and the velocity gradient at the wall becomes much
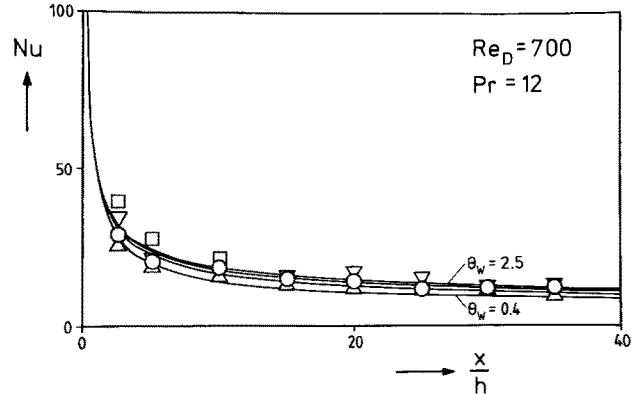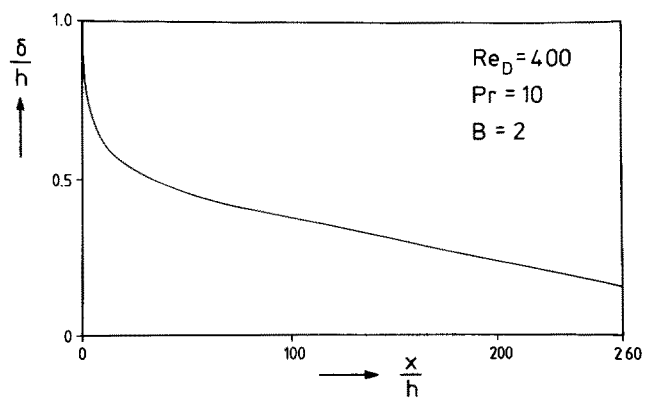
**Fig. 7.** Axial distribution of $\delta^*$ in the combined hydrodynamic and thermal entrance region
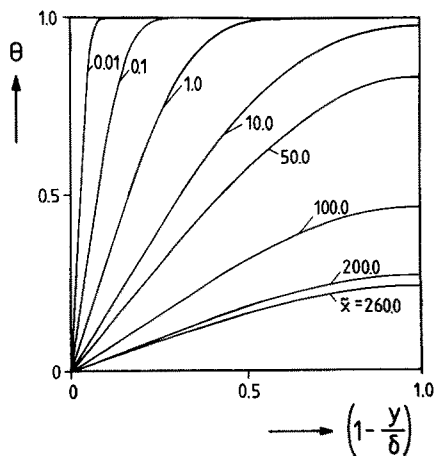
**Fig. 10.** Development of the temperature distribution in the combined hydrodynamic and thermal entrance region
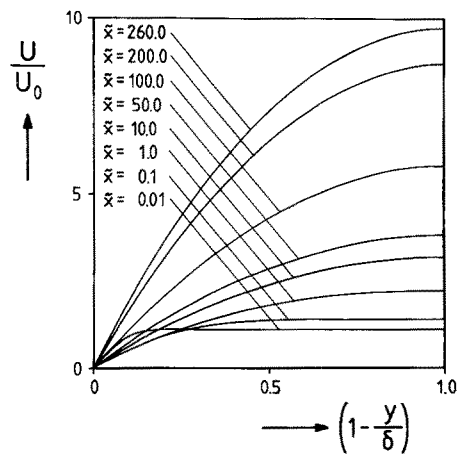
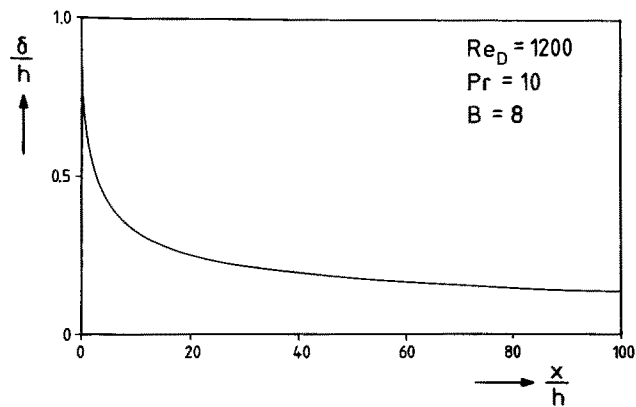**Fig. 8.** Development of $u/u_0$ in the combined hydrodynamic and thermal entrance region

**Fig. 11.** Axial distribution for $\delta^*$ in the combined hydrodynamic and thermal entrance region
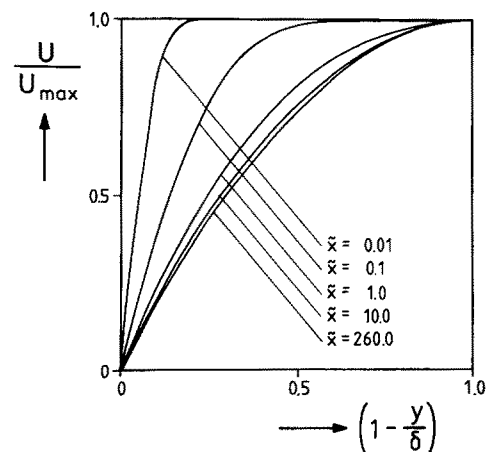
**Fig. 9.** Axial velocity distributions $u/u_{max}$ for various $x/h$ in the hydrodynamic and thermal entrance region
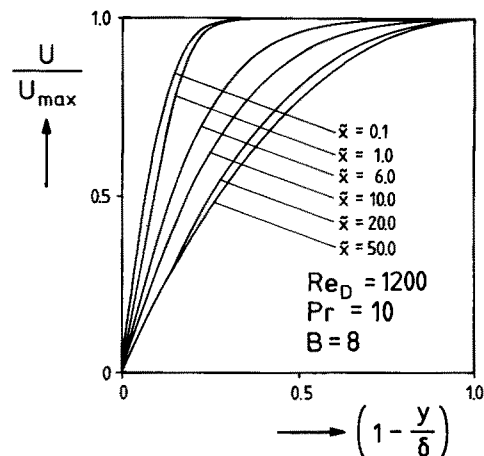
**Fig. 12.** Axial velocity distribution $u/u_{max}$ for various $x/h$ in the hydrodynamic and thermal entrance region

The temperature distribution for variable values of $\tilde{x}$ and for the ice layer characterized by Fig. 7 is shown in Fig. 10. With increasing $\tilde{x}$, the temperature at the centerline of the channel decreases, which can be accounted to the heat loss by wall cooling. For a larger value of the dimensionless freezing parameter, $B = 8$, and for a larger Reynolds number $Re_D = 1200$, the axial distribution of the ice-layer thickness is depicted in Fig. 11. In this case $\delta^*$ increases very rapidly for low values of $\tilde{x}$, whereas the ice-layer grows nearly linearly at larger values of $\tilde{x}$. Velocity profiles for this case under consideration are shown in Fig. 12. It can be seen that the distribution approaches a nearly parabolic profile for $\tilde{x} \approx 20.0$.

## 5 Concluding remarks

A simple numerical model was presented to predict the steady-state ice-layers at the cooled walls inside a parallel plate channel for arbitrary entrance velocity profiles. The numerical results were compared with experimental findings of Kikuchi [8] for the case of a fully developed entrance velocity profile and a generally good agreement was found. The model is flexible and can easily be extended by an appropriate turbulence model in order to calculate ice-layers at the cooled walls inside a parallel plate channel for arbitrary entrance velocity profiles and turbulent internal flow.

## References

1. Zerkle, R. D.: Sunderland, J. E.: The effect of liquid solidification in a tube upon laminar-flow heat transfer and pressure drop. J. Heat Transfer 90 (1968) 183–190
2. Özisik, M. N.; Mulligan, J. C.: Transient freezing of liquids in forced flow inside circular tubes. J. Heat Transfer 91 (1969) 385–390
3. Bilenas, J. A.; Jiji, L. M.: Numerical solution of a nonlinear free boundary problem of axisymmetric fluid flow in tubes with surface solidification. Proc. 4th Int. Heat Transfer Conf. 1 Paris. Amsterdam: Elsevier Publishing Company 1970 Cu 2.1 1–11
4. Chida, K.: Heat transfer in steady laminar pipe flow with liquid solidification. Heat Transfer: Jap. Res. 81 (1983) 81–94
5. Hwang, G. J.; Sheu, J. P.: Liquid solidification in combined hydrodynamic and thermal entrance region of a circular tube. Can. J. Chem. Eng. 54 (1976) 66–71
6. Lee, D. G.; Zerkle, R. D.: The effect of liquid solidification in a parallel plate channel upon laminar-flow heat transfer and pressure drop. J. Heat Transfer 91 (1969) 583–585
7. Cheng, K. C.; Wong, L. S.: Liquid solidification in a convectively cooled parallel-plate channel. Can. J. Chem. Eng. 55 (1977) 149–155
8. Kikuchi, Y.; Shigemasa, Y.; Ogata, T.: Steady-state freezing of liquids in laminar flow between two parallel plates. J. Nucl. Sci. Technol. 23 (1986) 43–55
9. Bennon, W. D.; Incropera, F. P.: Developing laminar mixed convection with solidification in a vertical channel. J. Heat Transfer 110 (1988) 410–415
10. Cebeci, T.; Chang, K. C.: A general method for calculating momentum and heat transfer in laminar and turbulent duct flows. Num. Heat Transfer 1 (1977) 39–68
11. Cebeci, T.; Bradshaw, P.: Physical and computational aspects of convective heat transfer. New York Berlin Heidelberg: Springer 1984

Prof. Dr.-Ing. H. Beer
Dipl.-Ing. B. Weigand
Institut für Technische Thermodynamik
Petersenstraße 30
6100 Darmstadt